2014 International Conference on Unmanned Aircraft Systems (ICUAS)
May 27-30, 2014. Orlando, FL, USA

Evaluation of Visual Servoing Control of Aerial Manipulators Using Test Gantry Emulation

Todd W. Danko and Paul Y. Oh

Abstract— **Unmanned Aerial Vehicles (UAVs) offer a means to vastly expand a manipulator's reach. Mounting an arm to a UAV greatly increases the utility of both the arm and the UAV.**

This paper describes the application of partitioning to control the redundant degrees of freedom of an emulated aerial manipulation system. Visual servoing is used to drive the end-effector pose relative to a target, treating relative motions between the host vehicle and target as perturbations. The position of the host platform, emulated by a gantry, is servoed using kinematic information from the manipulator in such a way that it enables the arm to return to a pose with a high degree of reachability while imposing minimal static torque on the host.

A prototype system is implemented and evaluated using a 6-DOF manipulator and a gantry in place of a flying UAV. The partitioning algorithm is exercised as a proof of concept motivating the future use of this approach on a flying platform, though further refinement is required before this goal may be realized.

I. Introduction

Applications of UAVs have evolved over time to provide valuable roles in intelligence, surveillance and reconnaissance for both civilian and military operations. The ability to closely inspect, manipulate or carry objects that they encounter could greatly expand the types of missions achievable by UAVs, likewise the ability to fly dramatically increases the work space of manipulators. High degree of freedom (DOF) robots with dexterous arms could lead to transformative applications such as infrastructure inspection and repair, law enforcement, disaster response, casualty extraction, and personal assistance, leading to a paradigm shift in the way UAVs are deployed. In this paper, such aerial manipulation systems are referred to as Mobile Manipulating Unmanned Aerial Vehicles (MM-UAV).

MM-UAV efforts are inspired by nature to implement truly dexterous manipulation from aerial vehicles in ways that are similar to how an octopus can use its tentacles to manipulate objects like seashells while hovering and "flying" over the ocean floor, vectoring jets of water to maintain dynamic stability.

The coordination of redundant degrees of freedom is demonstrated as humans seamlessly combine multiple degrees of freedom to track objects of interest. Small, quick motions are tracked by panning and tilting the eye, head motions often follow, allowing the eye to recenter to its straight ahead position while still tracking the object. A human can even become mobile to help track an object that is moving beyond the range of what is possible or comfortable using only eye or head motions.

Toward realizing this vision of MM-UAV, this paper describes an approach to use visual and kinematic sensing to coordinate motions of the redundant degrees of freedom of an aerial manipulation system. The main parts to this system are shown is Fig. 1 and include the host, which is a gantry used to emulate a UAV and a 6-DOF manipulator with an end-effector mounted camera. The goal of the manipulator is to maintain desired end-effector positions relative to objects of interest despite host platform or target motions. To accomplish this, the manipulator's degrees of freedom are visually servoed to a specified pose relative to a target while treating motions of the host platform or target as perturbations. Simultaneously, the host platform's degrees of freedom are servoed using kinematic information from the manipulator which is captured as the difference between the arm's current and "ready pose." To help the manipulator reject relative motions between the host and target, a ready pose is identified that allows the arm to easily move in any direction, compensating for such motions. Additionally, the arm's ready pose is selected so that the arm imparts minimal static torque on the host. A controller is used to drive the host to a position that allows the manipulator to return to this ready pose.

While the ultimate goal is to implement the algorithms described here on a flyable system, initial efforts make use of a gantry system to emulate the motions of a UAV [1], [2]. This gantry offers the benefits of experimental repeatability, easy access to ground truth information and the reduced potential for damaging equipment. Further, the gantry can, and is used as a shortcut that allows for certain parts of aerial manipulation systems to be focused on before mature approaches are available for the complete system. The implementation target is the Ascending Technologies Pelican [3] quadrotor which has an advertised payload of $650\ g$, however the authors of this paper have successfully flown a Pelican quadrotor while carrying a payload of $1\ kg$.

It is envisioned that a flying aerial manipulator based on the one being emulated here could be used for industrial inspection situations where a camera or other sensor must be positioned relative to objects of interest in confined spaces. While grasping with the manipulator is not addressed in this paper, the techniques described could be used to guide a gripper of an aerial manipulation system relative to an object of interest to facilitate grasping.

This work was supported in part by the National Science Foundation (NSF) award CNS-1205490. Any opinion, findings, and conclusions or recommendations expressed in this material are those of the authors and do not necessarily reflect the views of NSF.

Todd W. Danko and Paul Y. Oh are with the Drexel Autonomous Systems Laboratory, Drexel University, Philadelphia, PA 19104, USA {twd25, pyo22}@drexel.edu

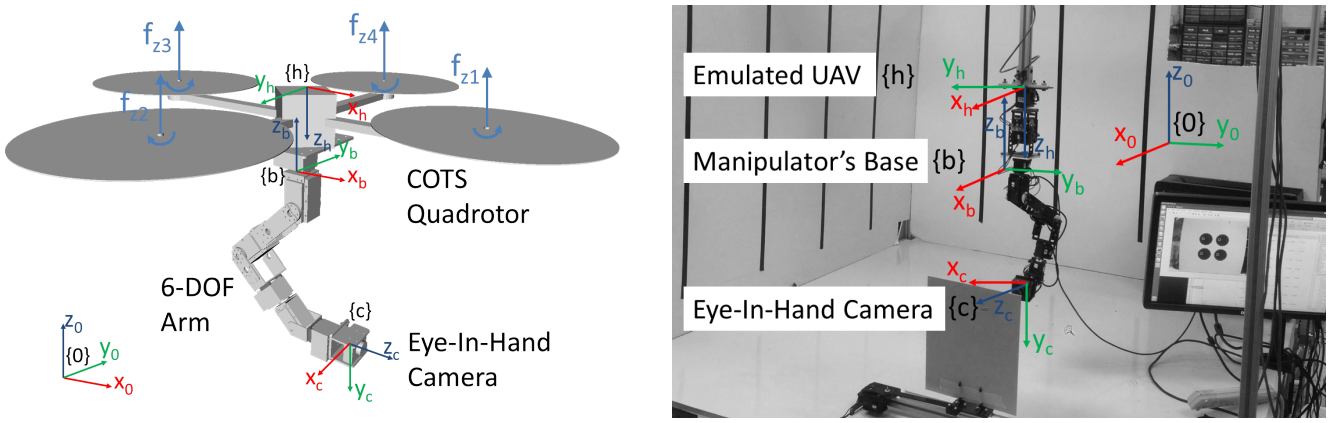

(a) MM-UAV Concept

(b) Surrogate Gantry

Fig. 1. A gantry is used to emulate a quadrotor UAV coupled to a six-DOF manipulator with eye-in-hand camera

The system would fly to the general region of interest under the guidance of GPS or other navigation aid. Upon arrival, the visual servoing would take over to guide the end-effector, which leads the way of the UAV to the desired goal position.

Section II of this paper examines literature related to manipulation from UAVs, the control of articulated aerial manipulation systems and visual servoing, including partitioning. Section III describes the approach to coordinated arm-host control as implemented on a test gantry. Section IV documents the characterization of the system as implemented on a gantry while Section V discusses a system demonstration. Finally, Section VI conveys conclusions and proposed future work.

II. Related Literature

A. Aerial Mobile Manipulation

Recent works [4], [5] have sought to apply ground-based mobile manipulation techniques to aerial vehicles. The Yale Aerial Manipulator can grasp and transport objects using a compliant gripper attached to the bottom of a T-Rex 600 RC helicopter [6]. Researchers at the University of Pennsylvania are using multiple quadrotors to cooperatively transport payloads using cables or grippers [7].

More recently, several groups have been investigating the use of articulated manipulators [8] as part of an aerial manipulation system, while [9] has evaluated the use of a Cartesian impedance controller for interaction tasks. The use of impedance control is attractive because it allows the manipulator to comply and compensate for unintended motions between the host platform and the environment.

Efforts under the Aerial Robotics Cooperative Assembly System (ARCAS) program demonstrated an approach to closely coordinate control of a quadrotor with a 3-link manipulator arm [10] while [11] described an approach for the coordinated control of a medium sized unmanned conventional helicopter and a redundant industrial manipulator that takes into account the kinematic coupling of the arm and host vehicle. Specifically, the authors designed an arm control strategy to mitigate an oscillation caused by a gyroscopic coupling of arm torques and body motions through the rotation of the main rotor of a conventional helicopter configuration. The counter-rotating propellers cancel out such oscillations on quadrotors such as those intended for this work.

B. Visual Servoing

The fundamental concept of Image Based Visual Servoing (IBVS) is that manipulator control is based on the minimization of an error in image feature space. To facilitate this, [12] described an interaction matrix, that is used to translate image feature position errors into desired motions of the camera. This approach is remarkably robust to inaccuracies in manipulator models, including undesirable relative motions between the object being tracked and the manipulator's base, making its application to UAVs attractive.

Numerous works [13]–[16] have explored the use of visual servoing to guide aerial vehicles, some even equipped with manipulators. None of these works, however, have considered the use of an eye-in-hand approach to regulate the pose of an articulated arm carried by an aerial platform. The value of such a configuration is robustness to perturbations to the pose of the host vehicle or target.

Visual servoing approaches generally calculate the desired rotational and translational velocities for the camera in a coordinated manner. This is based at the assumption that the degrees of freedom of the manipulator are equally adept at translating and rotating the camera in space, which is not true for most manipulators, and is especially not true when considering the redundant degrees of freedom of a MM-UAV system. A partitioning framework [17] was devised that uses frequency analysis to aid in the control law synthesis process, exploiting the kinematic and dynamic properties of each degree of freedom of a redundant system. In general, partitioning allows for the assignment of different roles to the degrees of freedom of a system in addition to using certain degrees of freedom as sensors for the control of others. In the original partitioning work, the authors used a pan-tilt

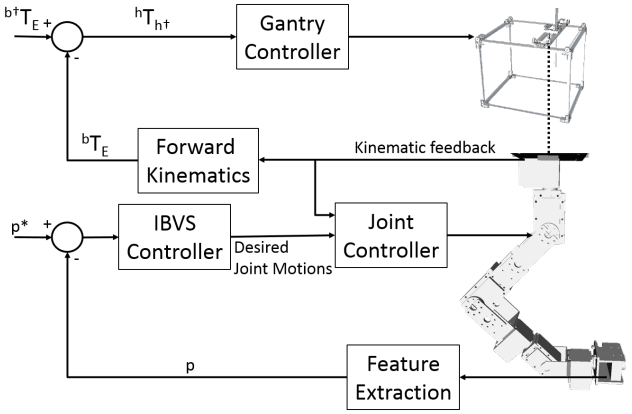

Fig. 2. Block Diagram of MIMO Controller

camera to track an object of interest, while a gantry moved the camera through space in an attempt to allow the camera to re-center it's pan and tilt angles. For partitioning to work properly, the degrees of freedom used as sensors should have the fastest response times for the system, while the benefit of the remaining degrees of freedom is that they provide a farther reach to the system.

III. System

The surrogate MM-UAV system (Fig. 1) consists of two main components, the manipulator arm, b, which is fit with an eye-in-hand camera, c, and the host platform, h. A prototype system was built that makes use of a manipulator attached to a gantry. A Multi-In-Multi-Out (MIMO) controller shown in Fig. 2 coordinates the motions of the arm and gantry.

The arm is servoed visually to maintain a desired camera pose, c^*, relative to a target, G, as described in Section III-B. The "*" notation indicates that this is a goal pose used for visual servoing. This is performed by calculating the desired camera motions and transforming them into joint angle motions to be executed by the manipulator.

The goal of the host, h, as described in Section III-D, is to position the arm's base, which is rigidly attached to the host, to a desired pose $b^\dagger$. The "†" notation indicates that this is a goal pose used for kinematic servoing. This pose is designed to allow the arm to return to a pose that maximizes the arm's reachability while minimizing static torque at the arm's base as described in Section III-C.

A. Manipulator

The Denavit-Hartenberg parameters that represent the six links of this arm are listed in Table I.

A lightweight camera is mounted to the arm's end-effector to provide an eye-in-hand visual servoing capability. The physical properties of the arm are listed in Table II. The as-built arm's mass is 932 g and has been successfully hovered and flown while mounted to a Pelican quadrotor.

Intermediate homogeneous transforms that represent each link are recreated from the Denavit-Hartenberg parameters using 1.

TABLE I
Denavit-Hartenberg Parameters

Link	θ (rad)	d (m)	a (m)	α (rad)
1	0	0	0	$-\pi/2$
2	0	0	l_3	0
3	0	0	0	$\pi/2$
4	0	l_4+l_5	0	$-\pi/2$
5	0	0	0	$\pi/2$
6	0	l_6+l_7	0	0

TABLE II
Physical Link Properties

Physical Link	Length (m)	Mass (kg)
l_1	0.041	0.102
l_2	0.055	0.185
l_3	0.148	0.233
l_4	0.103	0.147
l_5	0.042	0.087
l_6	0.072	0.113
l_7	0.055	0.065
Total:	0.516	0.932

$$
{}^{n-1}A_n(\theta_n) = \begin{pmatrix} \cos\theta_n & -\sin\theta_n\cos\alpha_n & \sin\theta_n\cos\alpha_n & a_n\cos\theta_n \\ \sin\theta_n & \cos\theta_n\cos\alpha_n & -\cos\theta_n\sin\alpha_n & a_n\sin\theta_n \\ 0 & \sin\alpha_n & \cos\alpha_n & d_n \\ 0 & 0 & 0 & 1 \end{pmatrix} \tag{1}
$$

The position of the end-effector can be described relative to the arm's base, ${}^bT_E$, as a series of transforms:

$$
{}^bT_E = \begin{array}{l} {}^bT_0\,{}^0A_1(\theta_1)\,{}^1A_2(\theta_2)\,{}^2A_3(\theta_3) \\ {}^3A_4(\theta_4)\,{}^4A_5(\theta_5)\,{}^5A_6(\theta_6)\,{}^6T_E \end{array} \tag{2}
$$

Where ${}^bT_0$ is the arm's fixed base transform and ${}^6T_E$ is the fixed transform from the manipulator's final link to the end-effector.

$$
{}^bT_0 = \begin{pmatrix} 1 & 0 & 0 & 0 \\ 0 & 1 & 0 & 0 \\ 0 & 0 & 1 & l_1+l_2 \\ 0 & 0 & 0 & 1 \end{pmatrix} \tag{3}
$$

$$
{}^6T_E = \begin{pmatrix} 0 & 0 & 0 & 0 \\ 0 & 1 & 0 & 0 \\ 0 & 0 & 1 & 0 \\ 0 & 0 & 0 & 1 \end{pmatrix} \tag{4}
$$

Inverse kinematics calculations are used to identify positions for each joint of the manipulator given a joint configuration $q = (\theta_1..\theta_6)$ that when executed, results in the end-effector reaching a desired pose. A standard closed-form inverse kinematics solver [18] is used for this six-DOF manipulator arm. Accordingly, eight kinematic configurations are often possible for each goal pose. A configuration is selected for execution based on its closeness to the previous arm configuration.

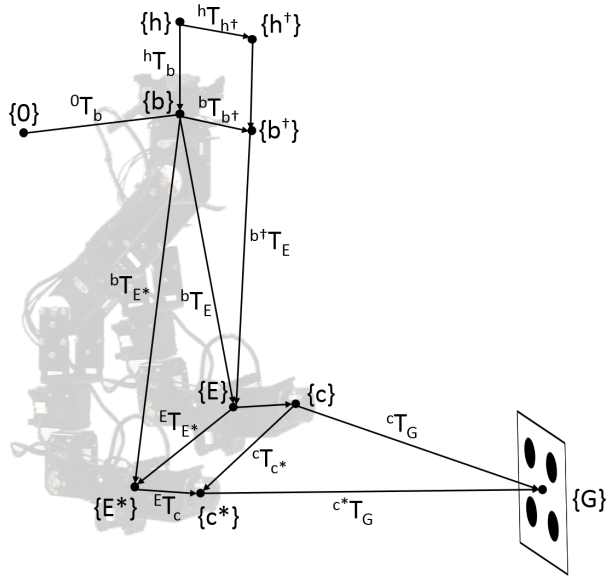

Fig. 3. Transforms between the world, 0, host, h, arm base, b, end-effector, E, camera, c and target, G

B. Visual Servoing

Eye-in-hand visual servoing controllers make use of a camera mounted to an end-effector to minimize the transform ${}^{c}T_{c^*}$ (Fig. 3) between a desired camera pose c^* and an observed one c relative to a goal target G.

The goal of IBVS [19] is to move features in image coordinates, p, to desired positions, p^*, by regulating motions of the camera. A square target with a known edge length of l_e is assumed. To position the camera such that its optical axis is perpendicular to the target plane, centered a distance z^* away, a synthetic target model p^* is created by calculating the positions of four points in image coordinates as shown in 5.

$$p^* = \begin{pmatrix} u_0 - a & v_0 + a \\ u_0 + a & v_0 + a \\ u_0 + a & v_0 - a \\ u_0 - a & v_0 - a \end{pmatrix} \tag{5}$$

Where u_0 and v_0 are the row and column center pixel of the image. a, as described in 6 accounts for the projection of the target onto the focal plane assuming a pin-hole camera model with a focal length of f and detector pitch of ρ.

$$a = \frac{f l_e}{2\rho z^*} \tag{6}$$

A pseudo-inverse of the interaction matrix L^+ [12] translates the motions from image space to the camera's coordinates and is calculated:

$$L^+ = \begin{pmatrix} c_1 & c_1 & c_1 & c_1 & -c_2 & c_2 & -c_2 & c_2 \\ -c_2 & c_2 & -c_2 & c_2 & c_1 & c_1 & c_1 & c_1 \\ -c_3 & c_3 & c_3 & -c_3 & c_3 & c_3 & -c_3 & -c_3 \\ -c_4 & c_4 & -c_4 & c_4 & 0 & 0 & 0 & 0 \\ 0 & 0 & 0 & 0 & c_4 & -c_4 & c_4 & -c_4 \\ c_5 & c_5 & -c_5 & -c_5 & c_5 & -c_5 & -c_5 & c_5 \end{pmatrix} \tag{7}$$

Where:

$$\begin{aligned} c_1 &= \tfrac{-\rho z^*}{4f}, c_2 = \tfrac{\rho z^{*3}\left(\frac{f^2+(f^2 l_e^2)}{4z^{*2}}\right)}{f^3 l_e^2}, \\ c_3 &= \tfrac{\rho z^{*2}}{4 f l_e}, c_4 = \tfrac{\rho z^{*2}}{f l_e^2}, c_5 = \tfrac{\rho z^*}{4 f l_e} \end{aligned} \tag{8}$$

The desired camera velocity $\dot{r}$ is then:

$$\dot{r} = L^+(p^* - p) \tag{9}$$

Which is then integrated over the control loop time step, t_s, to calculate an incremental camera motion ${}^{c}T_{c^*}$:

$${}^{c}T_{c^*} = \dot{r} t_s \tag{10}$$

The desired pose of the camera relative to the manipulator's base ${}^{b}T_{E^*}$ is simply an update to the camera's current pose modified by by the incremental motion ${}^{c}T_{c^*}$:

$${}^{b}T_{E^*} = {}^{b}T_{E}\,{}^{E}T_{c}\lambda_A\,{}^{c}T_{c^*}\,{}^{E}T_{c}^{-1} \tag{11}$$

Where λ_A is a fraction between 0 and 1 that represents the size of step toward the calculated goal to move during each time step. ${}^{b}T_{E}$ is the current position of the end-effector and is found using forward kinematics (2) and ${}^{E}T_{c}$ is the fixed transform between the end-effector and camera. An inverse kinematics solution is found that moves the arm to translate the end-effector toward ${}^{b}T_{E^*}$ and sent to the arm's actuators for execution.

C. Ready Pose Selection

In order to select a ready pose for the arm, two criteria are considered: reachability and the static torques created by the manipulator in a given pose. The ready pose is defined by a desired end-effector position with regard to the arm's base ${}^{b\dagger}T_{E}$.

Every manipulator has limitations in terms of the poses that the end-effector can reach. Analysis was performed using [20] to test how well this manipulator can reach finely spaced poses relative to the arm's base as shown in Fig. 4. To generate this reachability model, a discrete set of evenly spaced points was selected within a spherical volume that covers a workspace with a radius equal to that of the arm's extended length. For each point in this volume the inverse kinematics solver attempts to find a solution that would place the end-effector on the point at multiple different orientations. A point is considered to be more reachable if more orientations are solvable. As distance increases from the region of greatest reachability, fewer orientations are solvable. Ultimately points outside of the outer shell cannot be reached at all.

This reachability analysis shows that the arm has a "sweet-spot" (shown as red in Fig. 4) relative to the arm's base, where the arm is more likely to be able to achieve a desired pose.

The likelihood of achieving a given pose decreases as the end-effector's distance from this sweet spot increases. The selection of ${}^{b\dagger}T_{E}$ is based on several criteria. ${}^{b\dagger}T_{E}$ must be within the reachable workspace of the arm, but it will ideally result in an arm pose that induces minimal static torque on the host vehicle by the arm. To identify such a pose, static

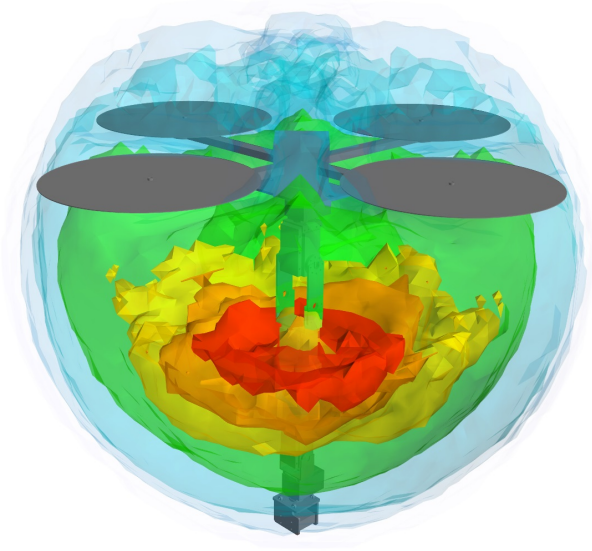

Fig. 4. Kinematic Reachability (Warmer Colors Indicate Greater Reachability)

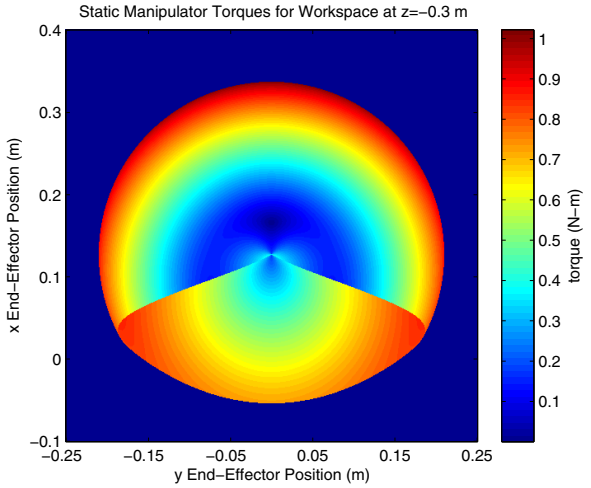

Fig. 5. Static Manipulator Torques for End-Effector Poses in The $z = -0.30\ m$ Plane

torques τ_m are iteratively calculated over the arm's reachable workspace using 12.

$$\tau_m(q) = \sum_{n=1}^{6} {}^{b}T_n(q)\,{}^{n}T_{CG_n} m_n g \tag{12}$$

Where ${}^{b}T_n(q)$ is the transform from the arm's base to the end of link n given joint configuration q, ${}^{n}T_{CG_n}$ is the transform from the end of link n to link n's center of gravity, m_n is the mass of link n and g is the acceleration due to gravity.

An end-effector orientation that is aligned with the host's x (forward) axis is maintained through these calculations based on the assumption that there is a preferred end-effector to target orientation and that vehicle motions should be used to help the end-effector reach this orientation.

A slice of the calculated torques in the plane at $z = -0.3$ m is shown in Fig. 5. It is desirable that the preferred arm pose impart minimal torque on the host vehicle and that the torques change smoothly as the end-effector pose varies around ${}^{b\dagger}T_E$. The discontinuity in the torque map shown in Fig. 5 is due to a change on the arm's kinematic configuration, for example, from elbow-up to elbow-down, in order to transition between two end-effector poses on opposite sides of the discontinuity.

D. Host Platform

This work focuses on the execution of camera positioning tasks in near-hover conditions and makes use of a surrogate gantry system to emulate such UAV motions. While this gantry is not a perfect substitute for an actual flying UAV, it is programmed to mimic the kinematics and dynamics of a quadrotor UAV.

Regardless of the use of a gantry or a flying UAV, the incremental position updates to the host are calculated by comparing the position of the end-effector relative to the arm's base ${}^{b}T_E$ with the desired pose of the end-effector relative to the arm's base ${}^{b\dagger}T_E$ to calculate ${}^{b}T_{b^\dagger}$. Since the arm's base, b, is rigidly fixed to the host, h, with a transform ${}^{h}T_b$, the desired incremental host motion is:

$${}^{h}T_{h^\dagger} = {}^{b}T_{b^\dagger} = \lambda_h\, {}^{b}T_E\, {}^{b\dagger}T_E^{-1} \tag{13}$$

Where λ_h is a proportional gain.

The motions described by ${}^{h}T_{h^\dagger}$ are transmitted to the gantry controller for execution. For the application to a flying UAV, desired position translations and yaw updates will be sent to the vehicle while roll and pitch will be controlled by the UAV's stability controller. Several works including [5], [10] describe approaches to control an aerial manipulation platform while accounting for the moving manipulator's static and dynamic impact on the systems center of gravity.

IV. Characterization

With the previously described arm mounted to a test gantry, the system was first characterized to help in the gain tuning process by moving a target on a linear motion platform in an approximate sinusoidal motion with increasing frequency over time along the host's y axis. The visual servoing system adjusted the position of the gantry and end-effector along the host's x, y, and z axes, though the performance characterization was performed using the system's y axis, as it was aligned with the axis of target motion.

One goal of this effort is to allow the arm to move to compensate for perturbations to the pose of the host. This is effectively a relative motion between the target and host so target motions can be treated as perturbations similarly to host motions relative to a fixed target. The dynamics of the target are such that moving the target makes it possible to replicate a greater range of frequencies for relative target-host motions than moving the gantry.

Three characterizations were performed. First, the gantry's gain was set to zero to allow for the characterization of the arm in isolation. Next, the gantry was characterized in isolation by zeroing out the arm's gain. It should be noted

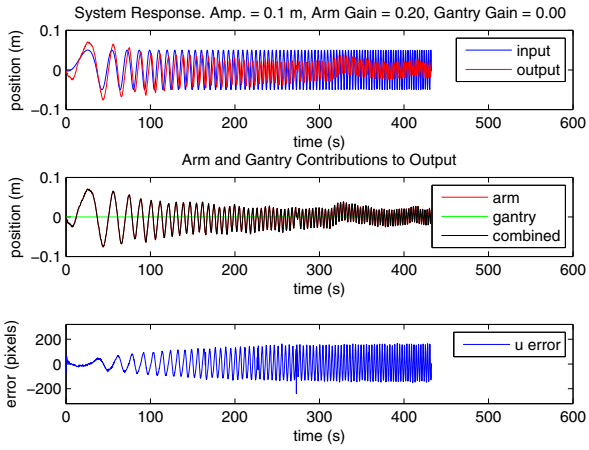

Fig. 6. System Response of Isolated Arm (Y Axis)

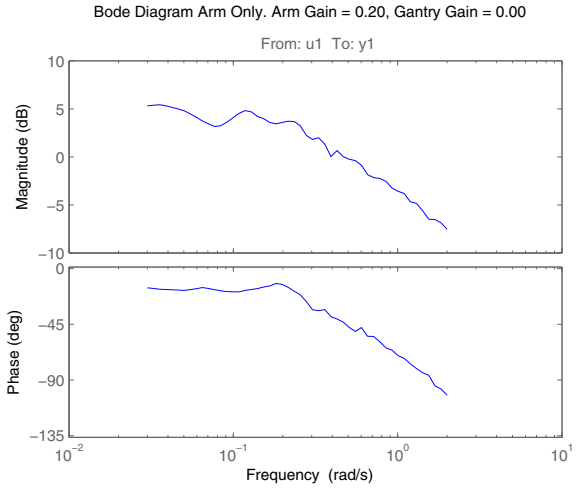

Fig. 7. Bode Diagram of Isolated Arm (Y Axis)

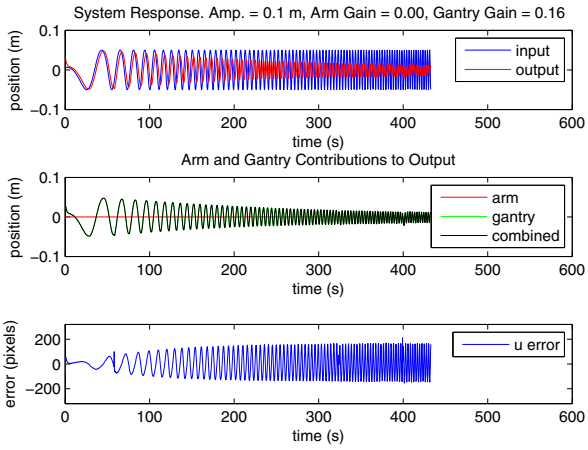

Fig. 8. System Response of Isolated Gantry (Y Axis)

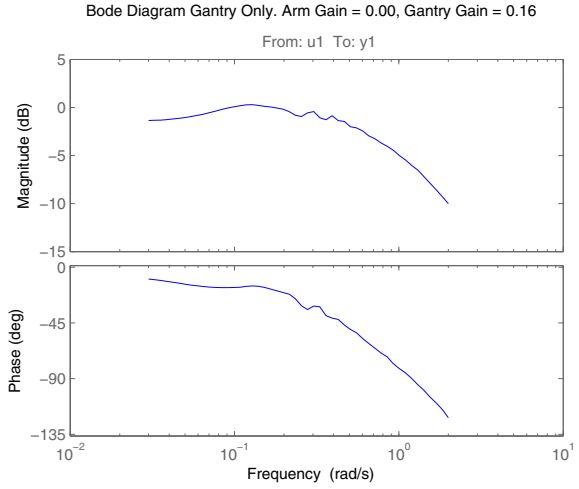

Fig. 9. Bode Diagram of Isolated Gantry (Y Axis)

that only for this second test, the gantry's input signal was provided by the camera because the arm was not moving to provide a signal based on it's pose. Finally, the combined system including the arm and gantry were characterized together with the gantry being servoed off of kinematic information from the visually servoed arm.

Figure 6 shows the isolated arm's response to an input motion along the arm's y axis, along with pixel error recorded through the camera while tracking the target. It can be seen that the system's output phase lag, which is primarily attributed to latency in image capture and feature extraction, increases along with attenuation with increased input frequency as shown in the accompanying Bode plot (Fig. 7). Figure 8 shows similar data for the gantry in isolation, while Fig. 9 is the corresponding Bode plot. It can be seen that the the arm alone has about twice the bandwidth than that of the gantry alone. Additionally, the system response time of the arm is approximately four times faster than the gantry. This is an important consideration for the application of partitioning where it is desirable for the faster degrees of freedom (the arm) to be used as sensors for the system's slower degrees of freedom (the gantry).

Figures 10 and 11 show performance of the combined system. The response time of the combined system is similar to that of the arm, though the degrees of freedom of the gantry provide a larger workspace than the arm would have statically mounted. The data shown in the Fig. 10 shows how the visually servoed arm leads the motions of the gantry and that gantry output attenuates with increased input frequency sooner than the arm. This is also illustrated in a series of images shown in Fig. 12. The combined system's overshoot at lower frequencies is attributed to the time it takes the end-effector to cross through the desired arm pose, ${}^{b\dagger}T_E$, while following the target, resulting in a delayed sign change for the gantry's input signal and subsequent reversal of gantry direction.

V. Demonstration

The system was demonstrated by having the end-effector servo to a specific pose relative to a static target placed in

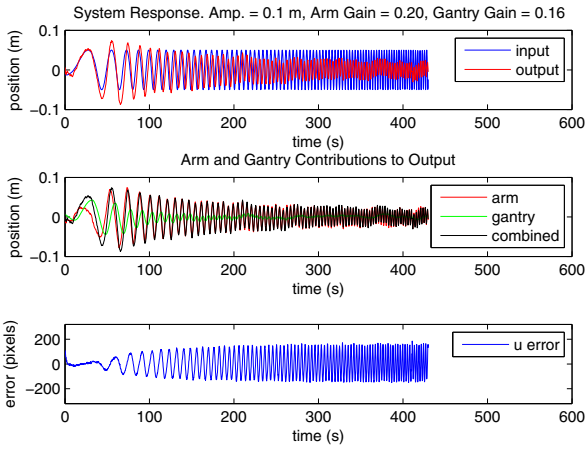

Fig. 10. System Response of Combined Arm & Gantry (Y Axis)

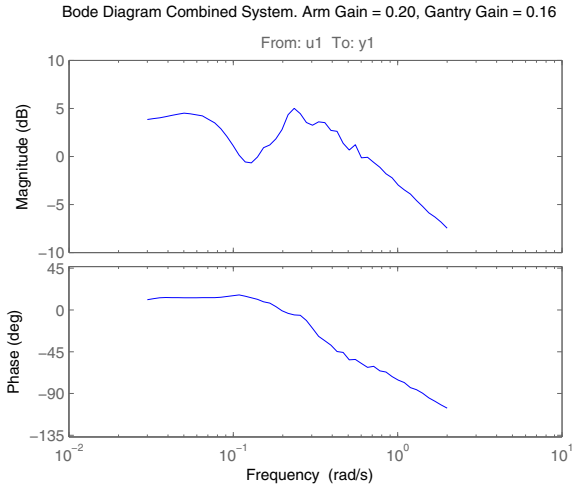

Fig. 11. Bode Diagram of Combined Arm & Gantry (Y Axis)

front of it. The paths of the gantry and camera in world coordinates as well as the camera relative to the arm's base are plotted along with the goal in world coordinates in Fig. 13. The motions of the arm seen at the 10 s mark are caused by the arm transitioning between an elbow-up and elbow-down configuration.

Figure 14 shows the input signal for the gantry ${}^{h}T_{h^{\dagger}}$ along with the resulting gantry position. Additionally, Fig. 15 shows the torques calculated around the arm's base y and x axis, induced by the arm's center of gravity displacement as the camera moves to different locations relative to the arm's base. The resulting torque change observed around the x axis during the arm's pose transition at 10 s is dramatic and serves as a motivation to investigate:

1) Restricting arm poses, preventing transitions from one kinematic configuration to another at the cost of a reduced reachable workspace
2) The use of an additional degree of freedom to allow smoother end-effector travel at the cost of additional weight

The steady state torques can be seen to settle close to 0 $N{\cdot}m$, which is expected because the arm has settled into it's ready pose which is designed to minimize such static torques.

VI. Discussion and Conclusions

These initial results show that this approach is worth further pursuit and will be expanded upon to ultimately create a flyable small MM-UAV system that uses visual servoing and kinematic feedback to position both the end-effector and UAV relative to a target.

A gantry was used as a starting point because it allows for the rapid prototyping of concepts, which can then be matured in preparation for flight. Simple proportional controllers were described in this paper along with a basic visual servoing approach. These simplifications are in place to allow for the evaluation of the partitioned control of the redundant DOFs of the host and arm. While making these simplifications facilitates rapid prototyping, they oversimplify the complexity of actual MM-UAV flight experiments. The gantry system allows for many hard problems to be abstracted away until solutions may be matured to a point that the entire system is flight worthy. The next steps toward implementing the desired MM-UAV system involve sequentially removing these simplifications by:

1) Evaluating the benefits of alternate control schemes for both the arm and host
2) Characterizing the dynamics of a quadrotor to obtain design criteria for a flyable manipulator arm
3) As necessary, lightening the arm and increasing the visual servoing execution loop rates to achieve an arm response time that is compatible with the selected quadrotor
4) Porting the system to a quadrotor that makes use of a motion capture system to aid state estimation
5) Improving the visual servoing technique to work with natural features
6) Transitioning to the use of the end-effector mounted camera to augment the quadrotor's inertial navigation system for state estimation, freeing the system from motion capture instrumented arenas

Beyond visually servoing the arm relative to a target, the use of the manipulator as a tactile sensor will also be explored. Coupled with a suitable compliant arm controller, this approach would allow the host platform to sense contact with the environment and adjust its pose to compensate even if the vision system can not see the collision or is otherwise unused.

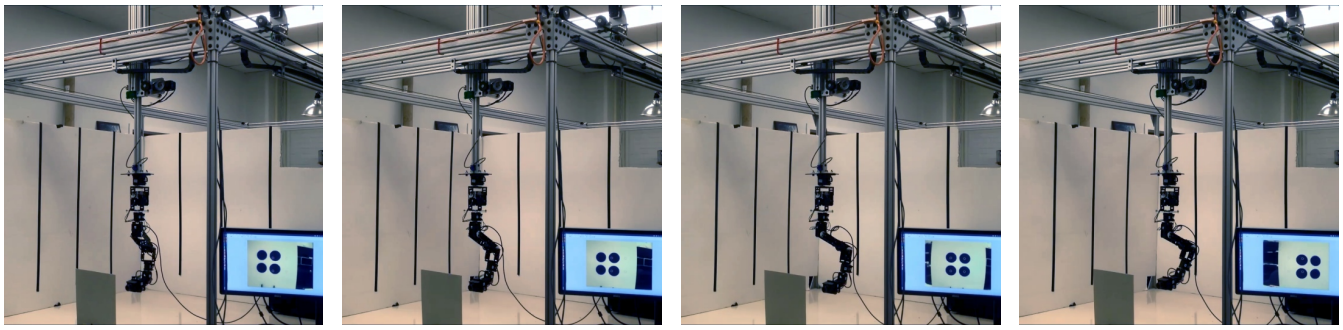

(a) Initial Pose (b) Arm Leading (c) Gantry & Arm Advancing (d) Arm Leading Return

Fig. 12. Visually servoed arm motions lead the gantry which is kinematically servoed off of the arm's pose

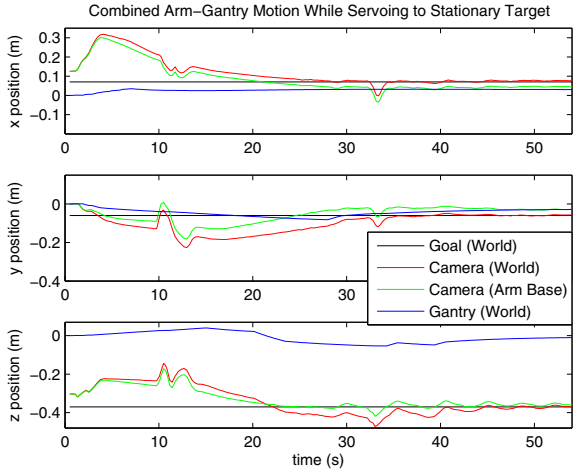

Fig. 13. Combined Arm-Gantry System Servoing to a Fixed Target

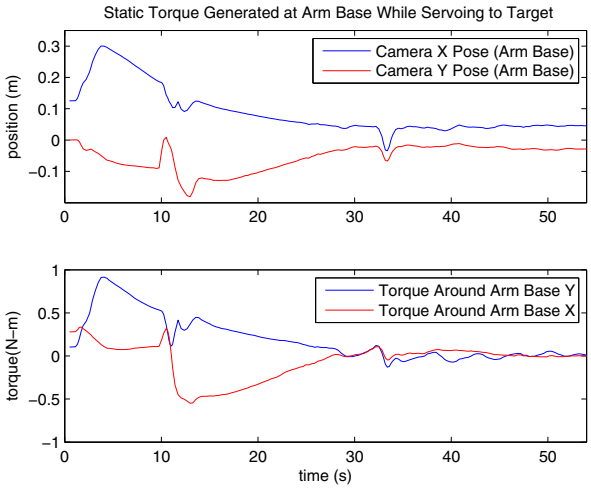

Fig. 15. Static Torques Generated by Center of Gravity Displacements

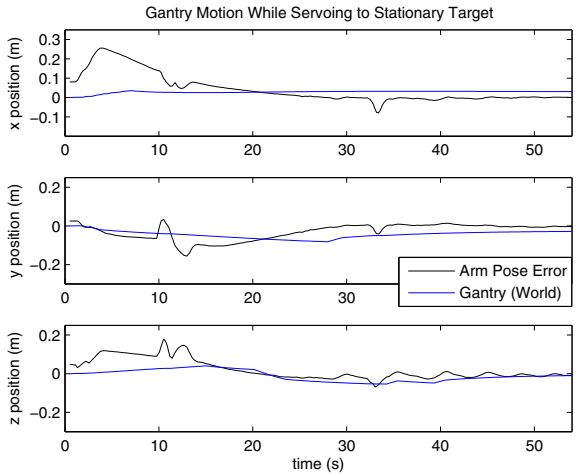

Fig. 14. Gantry Motions Based on the Difference Between Desired and Measured Host and Arm Base Position, ${}^{h}T_{h^{\dagger}}$

REFERENCES

[1] V. Narli and P. Y. Oh, "Hardware-in-the-loop test rig for designing near-earth aerial robotics," in *Robotics and Automation, 2006. ICRA 2006. Proceedings 2006 IEEE International Conference on*. IEEE, 2006, pp. 2509–2514.

[2] K. Sevcik and P. Oh, "Testing unmanned aerial vehicle missions in a scaled environment," in *Unmanned Aircraft Systems*. Springer, 2009, pp. 297–305.

[3] "Ascending Technologies pelican quadrotor," http://www.asctec.de/uav-applications/research/products/asctec-pelican, accessed: 2014-04-30.

[4] C. M. Korpela, T. W. Danko, and P. Y. Oh, "Mm-uav: Mobile manipulating unmanned aerial vehicle," *Journal of Intelligent & Robotic Systems*, vol. 65, no. 1-4, pp. 93–101, 2012.

[5] M. Orsag, C. Korpela, and P. Oh, "Modeling and control of mm-uav: Mobile manipulating unmanned aerial vehicle," *Journal of Intelligent & Robotic Systems*, vol. 69, no. 1-4, pp. 227–240, 2013.

[6] P. E. Pounds, D. R. Bersak, and A. M. Dollar, "Grasping from the air: Hovering capture and load stability," in *Robotics and Automation (ICRA), 2011 IEEE International Conference on*. IEEE, 2011, pp. 2491–2498.

[7] D. Mellinger, M. Shomin, N. Michael, and V. Kumar, "Cooperative grasping and transport using multiple quadrotors," in *Distributed autonomous robotic systems*. Springer, 2013, pp. 545–558.

[8] A. Torre, D. Mengoli, R. Naldi, F. Forte, A. Macchelli, and L. Marconi, "A prototype of aerial manipulator," in *Intelligent Robots and Systems (IROS), 2012 IEEE/RSJ International Conference on*. IEEE, 2012, pp. 2653–2654.

[9] V. Lippiello and F. Ruggiero, "Cartesian impedance control of a uav with a robotic arm," in *10th International IFAC Symposium on Robot Control*, 2012.

[10] A. Jimenez-Cano, J. Martin, G. Heredia, A. Ollero, and R. Cano, "Control of an aerial robot with multi-link arm for assembly tasks," in *IEEE Int. Conf. Robotics and Automation (ICRA), Karlsruhe, Germany*, 2013.

[11] F. Huber, K. Kondak, K. Krieger, D. Sommer, M. Schwarzbach, M. Laiacker, I. Kossyk, S. Parusel, S. Haddadin, and A. Albu-Schaffer, "First analysis and experiments in aerial manipulation using fully actuated redundant robot arm," in *Intelligent Robots and Systems (IROS), 2013 IEEE/RSJ International Conference on*. IEEE, 2013, pp. 3452–3457.

[12] F. Chaumette, P. Rives, and B. Espiau, "Positioning of a robot with respect to an object, tracking it and estimating its velocity by visual servoing," in *Robotics and Automation, 1991. Proceedings., 1991 IEEE International Conference on*. IEEE, 1991, pp. 2248–2253.

[13] L. Mejias, S. Saripalli, P. Campoy, and G. S. Sukhatme, "Visual servoing of an autonomous helicopter in urban areas using feature tracking," *Journal of Field Robotics*, vol. 23, no. 3-4, pp. 185–199, 2006.

[14] V. Ghadiok, J. Goldin, and W. Ren, "Autonomous indoor aerial gripping using a quadrotor," in *Intelligent Robots and Systems (IROS), 2011 IEEE/RSJ International Conference on*. IEEE, 2011, pp. 4645–4651.

[15] N. Kuntz and P. Y. Oh, "Towards autonomous cargo deployment and retrieval by an unmanned aerial vehicle using visual servoing," in *Proceedings of 2008 ASME Dynamic Systems and Controls Conference*, 2008.

[16] O. Bourquardez, R. Mahony, N. Guenard, F. Chaumette, T. Hamel, and L. Eck, "Image-based visual servo control of the translation kinematics of a quadrotor aerial vehicle," *Robotics, IEEE Transactions on*, vol. 25, no. 3, pp. 743–749, 2009.

[17] P. Y. Oh and K. Allen, "Visual servoing by partitioning degrees of freedom," *Robotics and Automation, IEEE Transactions on*, vol. 17, no. 1, pp. 1–17, 2001.

[18] L.-W. Tsai and A. P. Morgan, "Solving the kinematics of the most general six-and five-degree-of-freedom manipulators by continuation methods." ASME, 1985.

[19] B. Espiau, F. Chaumette, and P. Rives, "A new approach to visual servoing in robotics," *Robotics and Automation, IEEE Transactions on*, vol. 8, no. 3, pp. 313–326, 1992.

[20] R. Diankov and J. Kuffner, "Openrave: A planning architecture for autonomous robotics," *Robotics Institute, Pittsburgh, PA, Tech. Rep. CMU-RI-TR-08-34*, p. 79, 2008.